Journal of King Saud University – Science 32 (2020) 2397–2405

Contents lists available at ScienceDirect

Journal of King Saud University – Science

journal homepage: www.sciencedirect.com

Original article

Waste PET plastic derived ZnO@NMC nanocomposite via MOF-5 construction for hydrogen and oxygen evolution reactions

Mohd Ubaidullah [a], Abdullah M. Al-Enizi [a,*], Shoyebmohammed Shaikh [a], Mohamed A. Ghanem [a], Rajaram S. Mane [b]

[a] Department of Chemistry, College of Science, King Saud University, Riyadh 11451, Saudi Arabia
[b] Center for Nanomaterials & Energy Devices, School of Physical Sciences, S. R. T. M. University, Nanded (MS) 431606, India

ARTICLE INFO

Article history:
Received 19 February 2020
Revised 13 March 2020
Accepted 15 March 2020
Available online 24 March 2020

Keywords:
Waste PET plastic
Metal organic frameworks
Nanocomposite
Electro-catalysis
Energy

ABSTRACT

Waste PET plastic is the main solid waste to deteriorate the environment. Herein, we have utilized waste PET plastic to synthesize nitrogen doped mesoporous carbon functionalized zinc oxide (ZnO@NMC) nanocomposite through MOF-5 construction by low temperature solvothermal method for the first time. As per current energy needs, sustainable hydrogen production through water splitting is the modern appealing solution across the globe. The existence of carbon and nitrogen in ZnO@NMC nanocomposite were confirmed by several analytical techniques i.e. XRD, FTIR, CHN, and XPS. High specific surface area of (939 m^2/g) and *meso*-porosity (pore radius ~25 Å) may offer large number of active sites and easy charge relocation for hydrogen and oxygen evolution reactions via electro-catalysis. The prepared ZnO@NMC nanocomposite exhibits enhanced electro-catalytic activity for HER and OER in 0.5 M KOH solution. Tafel slope and over-potential (η_{10}) of ZnO@NMC nanocomposite were found to be ~108 mV/dec and 0.39 mV, correspondingly, for HER in 0.5 M KOH. ZnO@NMC nanocomposite also shows efficient OER electro-activity with Tafel slope and over-potential (η_{10}) of ~318 mV/dec and ~0.57 V respectively. ZnO@NMC nanocomposite shows better electro-catalytic performance compared to the reported pure ZnO nanostructures. Moreover, the constancy test was also checked through chrono-amperometry (CA) at fixed potential.

1. Introduction

The exhaustion of non-renewable fuels clues to the chase of smart renewable energy resources of high efficiency. The electro-catalysts made of noble metal oxides show wide range of electro-catalytic activity for hydrogen evolution reaction (HER) and oxygen evolution reaction (OER) (Ahmed and Mao, 2016; Cherevko et al., 2016). However, noble metals cannot be used commercially due to high cost. Economical, stable, efficient and active electro-catalysts are essential to overcome the scarcity of desirable electro-catalysts for HER and OER reactions. Among all energy resources, hydrogen can be considered as the most hopeful clean energy resource, because of high energy density and zero carbon emission (Abe et al., 2019; Jain, 2009; Nojoumi et al., 2009). Extraordinary combustion rate (1.4×10^8 J/kg, roughly 2788 times that of methane) of hydrogen and nonhazardous combustion product (H_2O) makes it important. Water splitting through electrochemical process is a smart and promising approach to produce hydrogen and oxygen (Elakkiya et al., 2019; Fester et al., 2018; Peng et al., 2007; Zou and Zhang, 2015). Numerous attempts was used to synthesize cheap transition metal oxides based electrocatalyst for HER and OER but it is still a challenge (Meyer et al., 2015; Peng et al., 2019; Sun et al., n.d.). At present, low cost electrocatalysts based on transition metal compounds for instance oxide, hydroxide, carbides, sulfides, borides, selenides, phosphide, nitrides, oxyhydroxides, phosphates and alloys getting immense attention (Carenco et al., 2013; Meyer et al., 2015; Read et al., 2016; Suen et al., 2017; Zou and Zhang, 2015).

This is well recognized that ZnO is an adoptable/compatible materials which hold high sensitivity, high electronic mobility, extraordinary surface area, non-toxicity, chemical and thermal

* Corresponding author.
E-mail addresses: mtayyab@ksu.edu.sa (M. Ubaidullah), amenizi@ksu.edu.sa (A. M. Al-Enizi).

Peer review under responsibility of King Saud University.

Production and hosting by Elsevier

https://doi.org/10.1016/j.jksus.2020.03.025

stability etc (Chen et al., 2012; Mohan et al., 2012; Qi et al., 2017; SoYoon et al., 2014; Theerthagiri et al., 2018). The features of ZnO materials can be tailored by changing the band gap for different applications such as electronic, optoelectronic, sensors, catalysts (Ahmad et al., 2020; Hwang et al., 2016; Khatoon et al., 2013; Kumar et al., 2018; Lehr et al., 2012; Yoo et al., 2020), piezoelectric (Nour et al., 2017), and energy harvesting (Kumar and Kim, 2012; Rahman et al., 2018). The doped/undopped ZnO were also reported as photo-catalysts for HER (Bera et al., 2018; Gao et al., 2013; Hwang et al., 2016; Su et al., 2018). Few reports are available in literature on electrochemical HER and OER using pure ZnO and ZnO composites (Desai et al., 2019; Hüner et al., 2018). In this article, we report the fabrication of hetero atom (N) doped mesoporous carbon functionalized ZnO (ZnO@NMC) nanocomposite via MOF-5 for electrochemical water splitting to HER and OER. The synthesized nanocomposite was methodically characterized. The electrochemical measurements of ZnO@NMC nanocomposite for HER and OER were investigated in details at room temperature.

2. Experimental

2.1. Materials

The following analytical grade reagents were used in the synthesis of nanocomposite without further refinement: $Zn(NO_3)_2 \cdot 6H_2O$, (98%, Aldrich), benzene-1,4-dicarboxylic acid (BDH, PET plastic derived), N, N-methyl formamide (DMF, 99%, Acros Organics), triethyl amine (TEA, BHD chemicals), ethylene glycol (BDH, chemicals), N-Methyl-2-pyrrolidone (NMP, Aldrich), Nafion (Aldrich) and potassium hydroxide (KOH, ≥85%, BDH, chemicals).

2.2. Depolymerization of waste PET plastic to produce organic linker (1, 4 benzene dicarboxylic acid/terephthalic acid/BDC)

Waste PET plastic were collected from the trash and washed thoroughly using distilled water, and then cut into small pieces. 10 g of waste PET plastic chips were kept in a 500 ml Teflon auto-clave reactor with 100 ml EG and 120 ml double distilled water, and then treated at 180 °C for 5 hrs. Then, the reactor left for cooling to room temperature (27 °C). Moreover, the resultant products were centrifuged and washed twice with ethanol, then dried at 100 °C for 20 hrs. FTIR analysis confirmed that the waste PET plastic produced BDC illustrates the same characteristics peaks at nearly similar IR bands of commercial purchased BDC (98%, BDH) (Fig. S1). Characteristic peaks corresponding to aromatic rings were observed at 730 cm^{-1} and 1680 cm^{-1}, whereas peaks corresponding to carboxylic groups were at 1290, 1420, 2542, and 2657 cm^{-1}. This suggests that the obtained product was indeed BDC as proved by the resemblance of the spectrum when compared to that of commercial BDC from BDH chemicals company.

2.3. Synthesis of MOF-5 by using waste PET plastic derived organic linker (BDC)

MOF-5 was synthesized by solvothermal route using a Teflon-lined high-pressure reactor. In a beaker, 12.0 mmol of $Zn(NO_3)_2 \cdot 6H_2O$ and 4.0 mmol of 1,4-benzen dicarboxylic acid (BDC, waste PET plastic derived) were mixed with 120 ml of dimethyl formamide (DMF) and 2 ml of triethyl amine (TEA) under continuous stirring and then transferred to Teflon reactor. The resulting mixture was heated at 100 °C for 20 h under autogenous pressure. Reactor was allowed to cool to 27 °C and the crystals of MOF-5 were collected via centrifugation process (8000 rpm for 20 min) and washed 3 times with DMF and then dried at 80 °C for 12 h in vacuum oven.

2.4. Carbonization of MOF-5

The resulting MOF-5 was carbonizedin the flow of nitrogen gas at 600 °C for 4 h. ZnO was formed owing to the decomposition of the MOF-5 framework between 250 and 520 °C as observed in the TG measurement (Fig. S2) (Liu et al., 2008). It is well known that at temperature higher than 800 °C, ZnO can reduce Zn (Liu et al., 2008) and subsequently, Zn metal (boiling point 908 °C) can be vaporized awayalong with the gas. Finally, the black colored powder obtained (at 600 °C) and referred to as ZnO@NMC (NMC = Nitrogen doped mesoporous carbon) nanocomposite.

2.5. Characterization techniques used

The obtained ZnO@NMC nanocomposite was further characterized using a variety of analytical techniques and then used by means of the electro-catalysts in electrochemical water splitting reactions for HER/OER (See. scheme 1). Morphology, surface texture and shape/size studies of the ZnO@NMC nanocomposite were examined through FE-SEM (JEOL JSM-7600F), HR-TEM (JEOL JEM 1400). SAED was also accomplished for crystallographic electron diffraction patterns of the materials. For HR-TEM study, ZnO@NMC nanocomposite was sonicated in ethanol through probe sonicator. Small quantity of the dispersed sample was put onto Cu-grid. The elemental analysis was conducted with CHN instruments (ICP-OES) to confirm the elements present in nanocomposite. P-XRD technique was employed to analyze the phase purity and crystallinity of the ZnO@NMC nanocomposite (Rigaku D/Max 2550 VB/PC). Furrier transform infra-redspectra of ZnO@NMC nanocomposite was captured through Bruker Tensor 27 FTIR instrument. The detailed porosity and surface area analysis were checked through Brunauer-Emmett-Teller (BET) (ASAP 2020, Micromeritics USA) at 77 K in liquid nitrogen. To estimate the BET surface area in

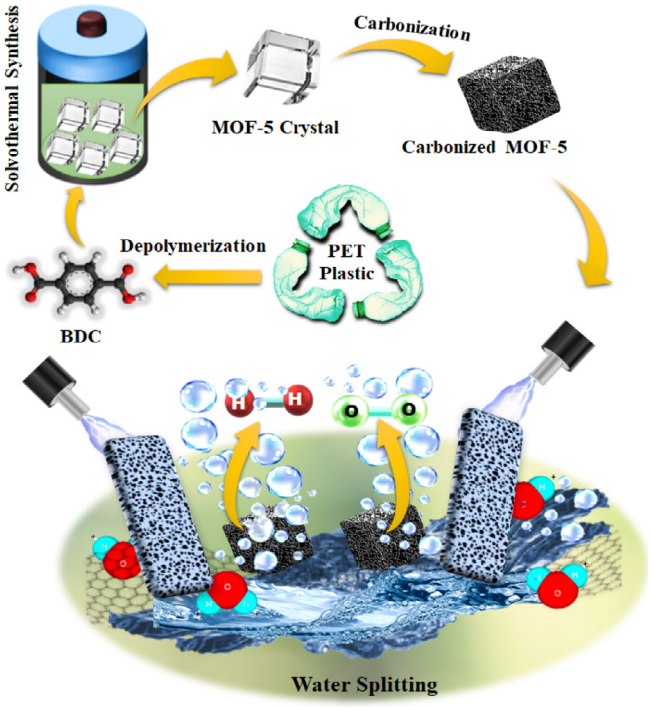

Scheme 1. Reaction scheme for solovo-thermal synthesis of ZnO@NMC nanocomposite for HER and OER activity.

the (P/P0) range of 0.05 to 0.35, a multipoint BET equation used while porosity were calculated via Barrett-Joyner-Halenda (BJH) and Dubinin-Astakhov (DA) methods. CHI-660E electrochemical work station was used to study the electrochemical activity of ZnO@NMC nanocomposite for water splitting to HER and OER at room temperature. The slurry for working electrode was made by taking powder sample and PVDF in the weight ratio of 90:10 with a small amount of (NMP) solution followed by stirring for 20 min. The prepared slurry was pasted on the glassy carbon electrode (i.e. working electrode). Pt-wire and Ag/AgCl electrodes were regarded as counter and reference electrodes correspondingly. Cyclic voltammetry (CV) and linear sweep voltammetry were accomplished at various scan rates for HER and OER in 0.5 M KOH versus Ag/AgCl. For stability test, chrono-amperometry (CA) measurements were also conducted at fixed potentials (i.e. at 0.7 and 0.8 V) for 300 s. Before preparatory the electrochemical measurements, the electrolyte was refined through a nitrogen purge for 5 min to eliminate the dissolved air from the electrolyte.

3. Results and discussion

SEM studies of MOF-5 (before and after carbonization) were depicted in Fig. 1. A well-defined smooth surface with cubic dense

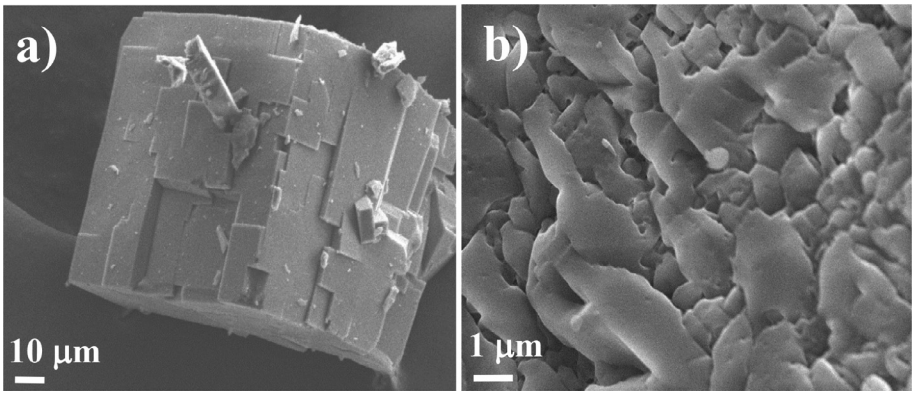

Fig. 1. FE-SEM images of MOF-5 (a) Before carbonization (b) After carbonization.

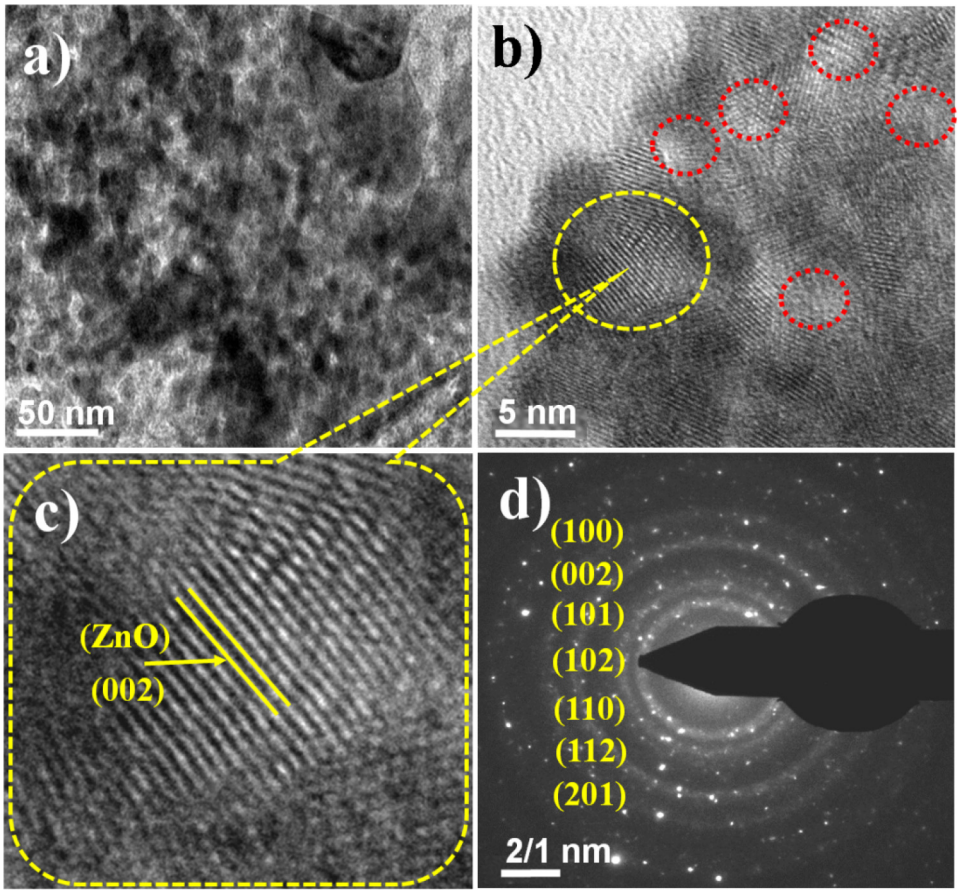

Fig. 2. HR-TEM Studies of ZnO@NMC composite (a) TEM micrograph (b) HR-TEM micrograph (c) Spatial distribution at high resolution and (d) SAED patterns.

structure of MOF-5 was observed before carbonization. A careful visualization of SEM studies reveals that it composed of agglomerated cube shaped particles as shown in Fig. 1a.

Whereas; after carbonization of MOF-5, the big and dense cube collapsed with mesoporous nanocomposite materials (Fig. 1b) (Yang et al., 2018). TEM studies of the nanocomposite also reveal the agglomeration of cube shaped particles with small extent (Fig. 2a). Fig. 2b represents the HR-TEM study of the nanocomposite, which clearly shows the development of lattice fringes of ZnO nanoparticles as well confirmed by XRD studies. These fringes were closely observed at high resolution and indexed with ⟨1 0 1⟩ plane of ZnO crystal lattice with d-spacing of 0.242 nm (Fig. 2c). The analyzed results are in good agreement with JCPDS#75–1526 having hexagonal wurtzite crystal structure of ZnO. The red circles marked in Fig. 2b showed the mesoporous nature of the materials. Fig. 2d shows the SAED pattern of the nanocomposite which was indexed to (1 0 0), (0 0 2), (1 0 1), (1 0 2), (1 1 0), and (1 0 3) planes of ZnO phase and corroborated well with the XRD diffraction pattern of ZnO@NMC nanocomposite.

Before carbonization of MOF-5, X-ray diffraction patterns was recorded and establish a perfect match with the existing XRD data of MOF-5 as depicted in Fig. S3. After carbonization of MOF-5, the phase and crystal structure of the prepared ZnO@NMC nanocomposite have also been investigated by P-XRD studies (Fig. 3a). The diffraction patterns were indexed at 2θ of 31.9°. 34.7°,36.2°, 47.6°, 56.6°, 63.1°, 67.9° and 69.0°, which were well correlated with the ZnO lattice planes of (1 0 0), (0 0 2), (1 0 1), (1 0 2), (1 1 0), (1 0 3), (1 1 2) (2 0 0) and (2 0 1) (JCPDS#75–1526) (Carenco et al., 2013). The XRD results are perfectly corroborated with SAED studies. The characteristic carbon peak appeared at 2θ of 30° and the intense diffraction patterns indicate the high degree of crystallinity of the nanocomposite. Zero impurity phases were detected, which support the formation of ZnO@NMC nanocomposite. The chemical bonding and constituent element of ZnO@NMC nanocomposite were examined by FTIR spectroscopy. The absorption peaks below 1000 cm^{-1} in finger print region confirm the formation of metal oxides, which is because of inter atomic vibrations (Matinise et al., 2017). The broad band appears at ~3290 cm^{-1}- which corresponds to the —OH stretching. The bands at ~1590, ~1385 and ~1100 cm^{-1} are due to the C—C, C=O and C—O stretching vibration (Balaji and Sathish, 2014). The bands appear at ~876 and ~752 cm^{-1} belong to C-N stretching (Balaji and Sathish, 2014) as shown in Fig. 3b. The weak bands appear at ~670 and ~540 cm^{-1}, which were associated with Zn–O. TGA, was performed from 10 to 750 °C with heating rate 10 °C in N_2 environment to examine the thermal stability of MOF-5. Two weight losses were identified at 140 – 230 °C and 250 – 520 °C (Fig. S2). The first weight loss (~32%) attributed to the loss of solvents (DMF, TEF) accommodated in the cavities of MOF-5, though the second weight loss from 250 to 520 °C about (~58%) can be ascribed to the decomposition of metal organic frameworks and construction of ZnO nanoparticles. Therefore, calcination above 500 °C could be regarded to the formation of stable ZnO nanoparticles and carbon. Raman studies carried out to examine the degree of graphitization along with the crystallinity of ZnO@NMC nanocomposite. The bands labelled at ~1354 and ~1582 cm^{-1} belong D and G bands of ZnO@NMC nanocomposite (Fig. 3c). The intensity ratio of I_D/I_G bands was estimated ~1.12, which resemble to graphitic defects of D and G Raman bands of ZnO@NMC nanocomposite. The bands at ~573 and ~434 cm^{-1} belong to E_1 and E_2 mode of ZnO and the band at 331 cm^{-1} links with A_1 mode of ZnO (Callsen et al., 2011).

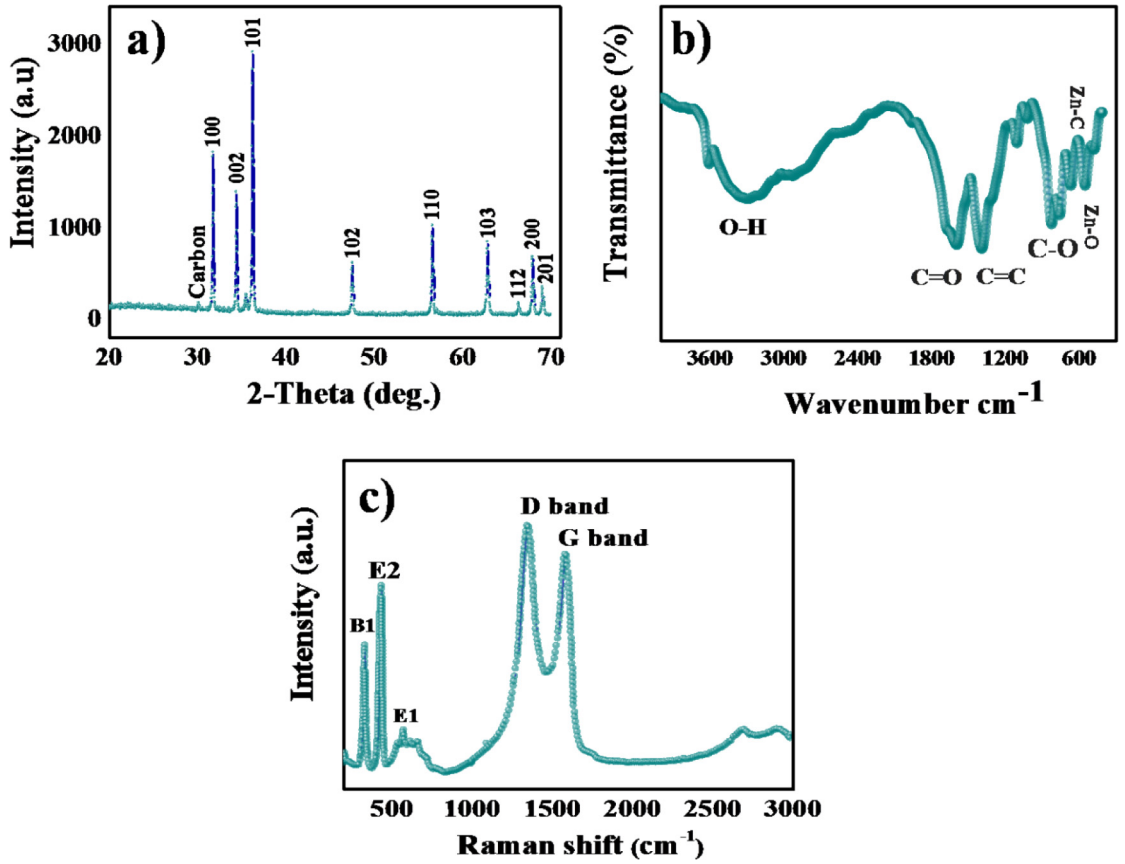

Fig. 3. (a) P-XRD pattern, (b) FTIR spectra (d) TGA plot (d) Raman spectra of ZnO@NMC composites.

CHN and ICP-OES studies were carried out to compute the C (35.15%), H (2.01%), N (8.73%), O (28.10%) and Zn (25.23%) in ZnO@NMC nanocomposites as given in table 1. The decent amount of nitrogen existing in C matrix, which also supports the electrical conductivity and the creation of massive amount of defects. The N_2 A-D isotherms studies were utilized to inspect the porosity and specific surface area of the prepared ZnO@NMC nanocomposites (Fig. 4a). ZnO@NMC nanocomposite exposes type-IV hysteresis loop, signifying the occurrence of mesoporous structure. The specific surface area 939 m^2/g was achieved (Fig. 4b), which is 75 times higher than that of the reported surface area of pure ZnO nanoparticles (12.4 m^2 g^{-1}) (Lonkar et al., 2016). The detailed BET results are composed in Table-S1. A BET table comprises of surface area and high surface area of ZnO@NMC nanocomposite produces the more surface-active sites directly related to the high performance of electro-catalytic activity in water splitting reactions. The BJH and DA studies was employed to examine the pore size parameters which found to be ~24–25 Å (Fig. 4c and 4d) respectively. The detailed information related to surface area of ZnO@NMC nanocomposite has been given in table 2.

Fig. S4 depicts the XPS survey of ZnO@NMC nanocomposite. The major peaks of Zn, O, N and C confirm the formation of nitrogen doped carbon supported ZnO (i.e. ZnO@NMC) nanocomposite. The deconvolution of Zn-2p bands indicate two symmetric peaks at 1026.42 and 1049.42 eV corroborated to $Zn2p_{1/2}$ and $Zn2p_{3/2}$ as shown in Fig. 5a. The O-1 s high resolution spectrum demonstrates three bands at 528.02, 531.31 and 535.35 eV (Fig. 5b). The peaks at 401.65, 403.53 and 405.14 eV can be ascribed to N1s (Fig. 5c). C-1 s spectrumat high resolution which can be fitted to three peaks with binding energies of 283.20, 284.42, and 285.88 eV as depicted in Fig. 5d. Finally we can conclude that the provided characterization results of the prepared materials strongly confirmed the formation of ZnO@NMC nanocomposite.

Electrochemical studies of ZnO@NMC were carried out for HER and OER using 0.5 M KOH electrolyte. Fig. 6a shows CV plot of ZnO@NMC in the potential window range from –2 to + 1 V versus Ag/AgCl in 0.5 M KOH at 50 mV/s. CV plot of ZnO@NMC shows bifunctional activity for HER and OER in cathodic and anodic regions, respectively. LSV plots of ZnO@NMC for HER at different scan rates are shown in Fig. 6b.

We observed that the ZnO@NMC generate high current density of ~90 mA/cm^2 at 50 mV/s with over-potential of 0.39 V at 10 mA/cm^2 in 0.5 M KOH. The over-potential of pure ZnO nanostructured materials at 10 mA/cm^2 was reported of ~0.80 V in alkaline medium for HER (Kwak et al., 2017). Fig. 6c shows Tafel plots of ZnO@NMC electro-catalysts for HER. Tafel slope is found to be ~108 mV/dec for HER. The Tafel slope of pure ZnO nanostructured

Table 1
CHN and ICP-OES analysis of ZnO@NMC nanocomposite.

Weight Percentage (%)					
Compound	C	H	N	O	Zn
ZnO@NMC	35.15	2.01	8.73	28.10	25.23

Table 2
Surface area porosity investigation (BET) of ZnO@NMC nanocomposite.

Surface Area and Porosity Investigation			
Compound	**Specific surface area (m^2/g)**	**BJH Pore Size (Å)**	**DA Pore Size (Å)**
ZnO@NMC	939	24	24.5

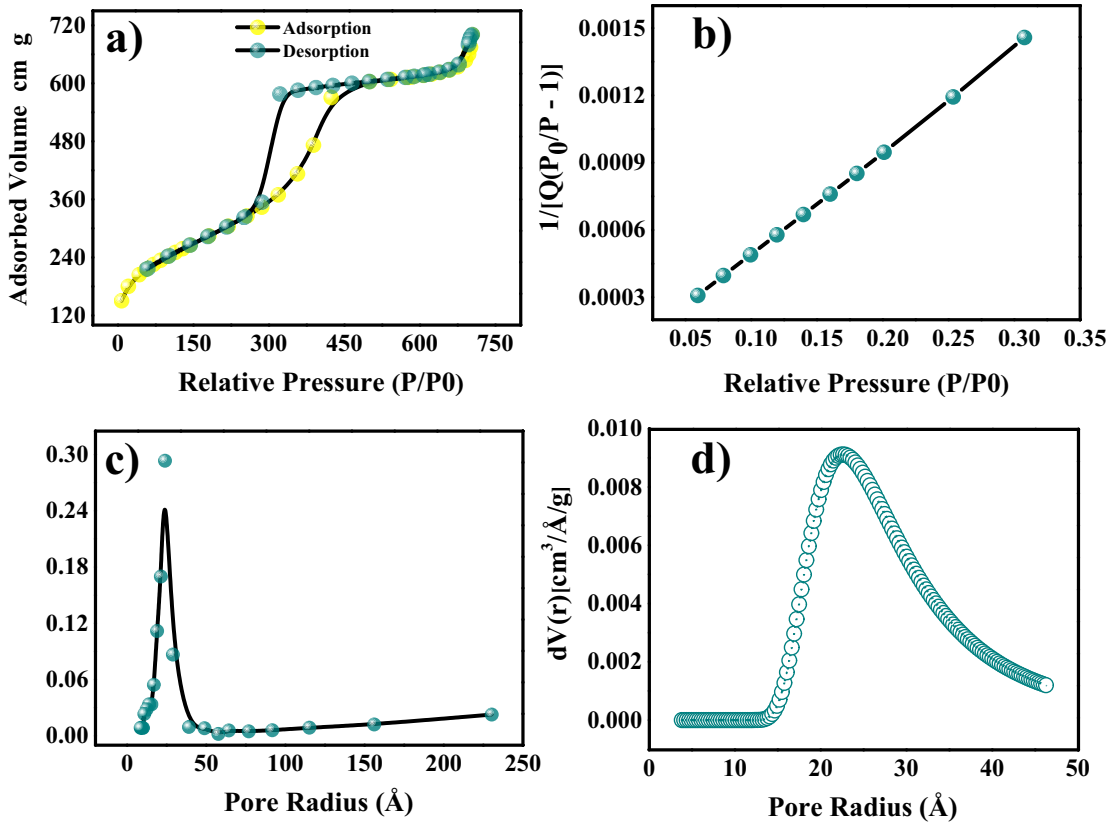

Fig. 4. Surface area porosity investigation (BET) of ZnO@NMC nanocomposite (a) N2 A-D isotherms (b) BET plot (c) BJH porosity plot and (d) DA porosity plot.

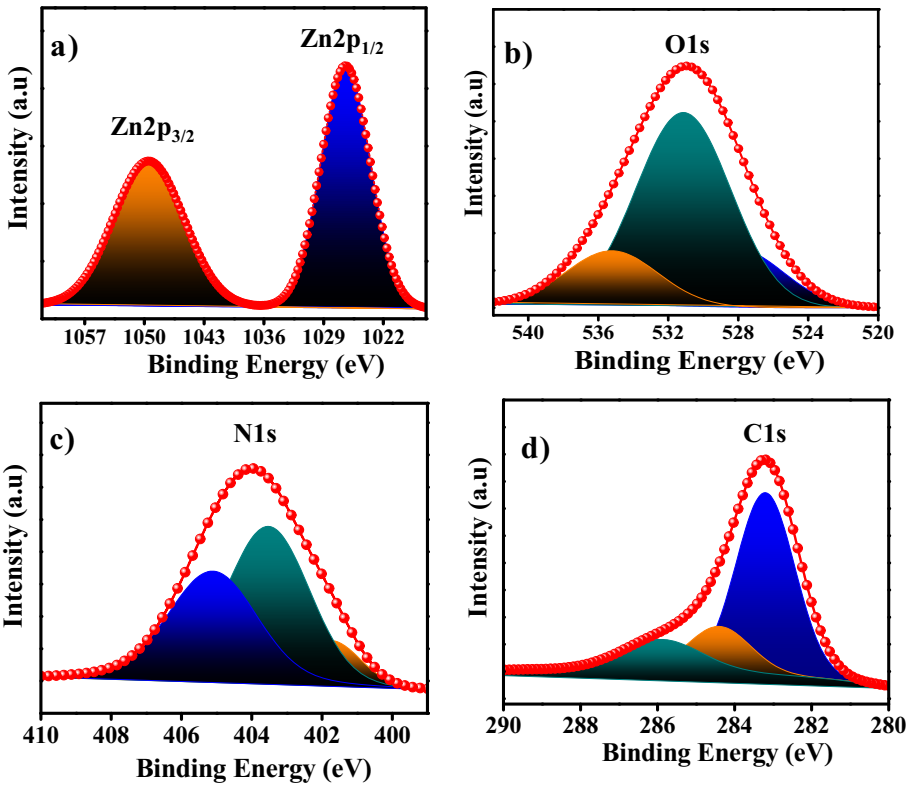

Fig. 5. XPS analysis of ZnO@NMC (a) XPS survey spectrum of ZnO@NMC (b) HR C1s spectrum (c) HR N1s and (d) HR Zn2p.

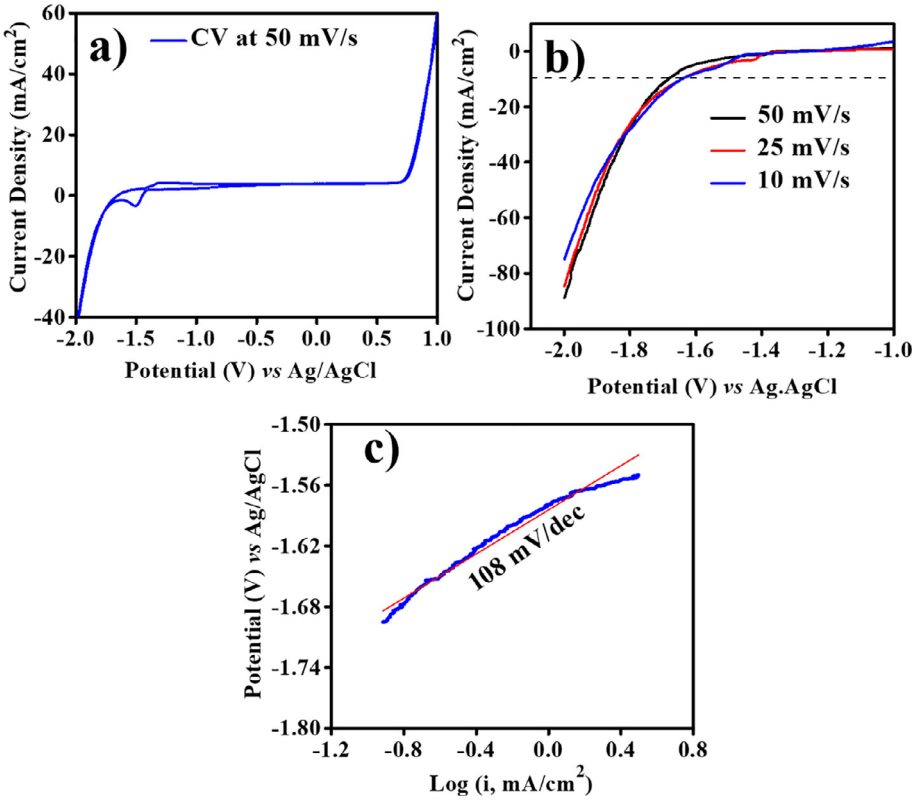

Fig. 6. (a) CV, (b) LSV for HER and (c) Tafel plots for HER of ZnO@NMC in 0.5 M KOH *Vs.* Ag/AgCl.

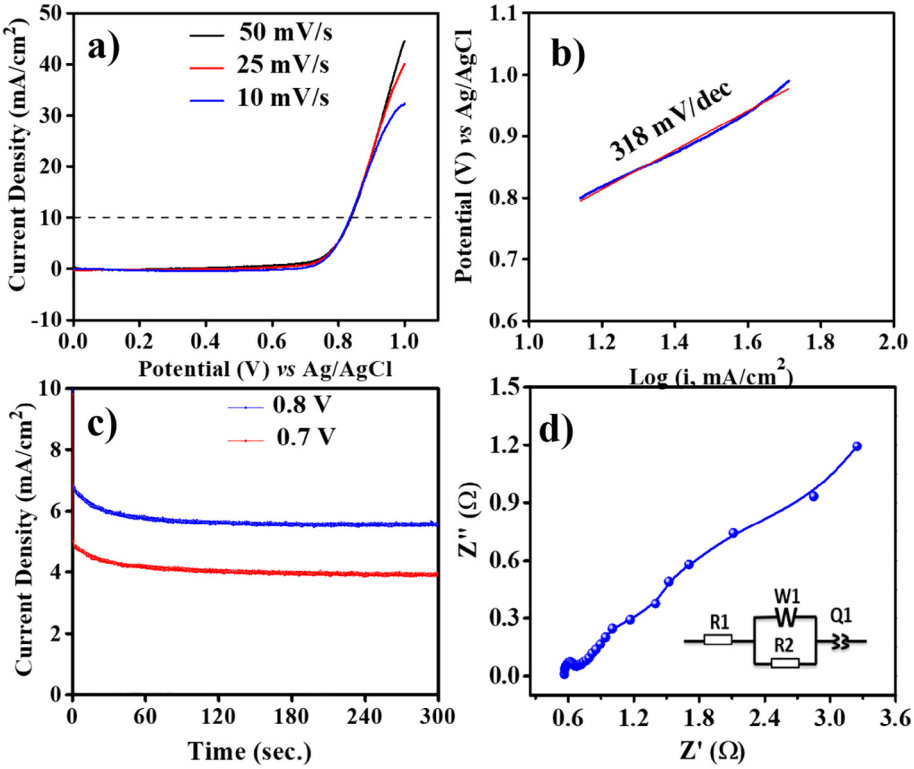

Fig. 7. (a) LSV for OER, (b) Tafel for OER, and (c) CA for stability test and (d) Impedance graph of ZnO@NMC in 0.5 M KOH *Vs.* Ag/AgCl.

materials was reported of ~210 mV/dec for HER in alkaline medium (Kwak et al., 2017).

In recent times, transition metal oxide nanorods are reported as superior electro-catalysts for HER with the Tafel slope value of ~135 mV/dec in 0.5 M KOH (Ahmed et al., 2019). Fig. 7a shows LSV plots of ZnO@NMC for OER using various scan rates. This is notable that the ZnO@NMC electro-catalysts also generate good current in anodic region with respect to the OER activity. The current density of ZnO@NMC electro-catalysts was observed to be ~48 mA/cm^2 at 50 mV/s. The over-potential of electrode materials was found to be ~0.570 V at 10 mA/cm^2 in 0.5 M KOH. Zinc based oxide nanobricks were reported as efficient electro-catalysts and the over-potential was reported of ~0.475 V at 10 mA/cm^2 using high concentration of alkaline electrolyte i.e. 1.0 M KOH (Alshehri et al., 2018). The over-potentials of transition metal oxides nanoparticles were also reported in the range from 0.35 to 0.97 V for the OER (Alajmi et al., 2018; AlShehri et al., 2017; Ling et al., 2014). IrO_2-ZnO and RuO_2-ZnO nanohybrids were reported as efficient OER electro-catalysts with over-potentials of ~0.5 V and 0.47 V, respectively, using 0.1 M KOH electrolyte (Kwak et al., 2017). Tafel plots of ZnO@NMC electro-catalysts for OER were shown in Fig. 7b. Tafel slope value of ZnO@NMC electro-catalysts for OER was found to be ~318 mV/dec. Fig. 7c shows CA plots of ZnO@NMC electrode materials for stability at fixed potential of 0.7 and 0.8 V for 300 s in 0.5 M KOH. A Nyquist plot of the as-prepared nanocomposite electrode is presented in Fig. 7d. A smallest real axis intercept (i.e., 0.60 Ω), indicating that is possesses the lowest charge transfer resistance, facilitating rapid charge transportation through electrode the material based on its unique morphology, which facilitate easy percolation of electrolyte ions for enhanced OER and HER activity. The greater charge transfers resistance values and lower charge mobility of and may not allow electrolytes ions to remain in chemical contact with electrode material surfaces, resulting in reduced catalytic activity. The stable nature of the electrode materials is one of the important parameters for electrolysis of water. CA results confirm that the ZnO@NMC electrodes generate stable current density with time at the fixed potentials. Based on the electrochemical results, we can suggest that the prepared ZnO@NMC electro-catalysis could be an alternative of efficient electro-catalysts in electrolysis of water for HER and OER.

4. Conclusion

Waste PET plastic (a major solid waste to environment) was utilized to synthesize novel high surface area containing ZnO@NMC nanocomposite through MOF-5 *via* simple solvothermal route for the first time. The prepared ZnO@NMC nanocomposite was characterized systematically using analytical techniques including electron microscopy, XRD, FTIR CHN, and XPS. ZnO@NMC nanocomposite exhibit 75 times higher surface area (939 m^2/g) compared to reported pure ZnO nanoparticles. ZnO@NMC nanocomposite demonstrates higher electro-catalytic activity for HER and OER with low Tafel slope and over-potential (η_{10}) values in alkaline medium than reported pure ZnO nanoparticles.

Declaration of Competing Interest

The authors declare that they have no known competing financial interests or personal relationships that could have appeared to influence the work reported in this paper.

Acknowledgements

This Project was funded by the National Plan for Science, Technology and Innovation (MAARIFAH), King Abdul Aziz City for Science and Technology, Kingdom of Saudi Arabia, Award Number (12-ENE-2893-02).

Appendix A. Supplementary data

Supplementary data to this article can be found online at https://doi.org/10.1016/j.jksus.2020.03.025.

References

Abe, J.O., Popoola, A.P.I., Ajenifuja, E., Popoola, O.M., 2019. Hydrogen energy, economy and storage: review and recommendation. Int. J. Hydrogen Energy 44, 15072–15086. https://doi.org/10.1016/j.ijhydene.2019.04.068.

Ahmad, I., Ahmed, E., Ahmad, M., Akhtar, M.S., Basharat, M.A., Khan, W.Q., Ghauri, M.I., Ali, A., Manzoor, M.F., 2020. The investigation of hydrogen evolution using Ca doped ZnO catalysts under visible light illumination. Mater. Sci. Semicond. Process. 105,. https://doi.org/10.1016/j.mssp.2019.104748 104748.

Ahmed, J., Mao, Y., 2016. Ultrafine Iridium Oxide Nanorods Synthesized by Molten Salt Method toward Electrocatalytic Oxygen and Hydrogen Evolution Reactions. Electrochim. Acta 212, 686–693. https://doi.org/10.1016/j.electacta.2016.06.122.

Ahmed, J., Ubiadullah, M., Alhokbany, N., Alshehri, S.M., 2019. Synthesis of ultrafine NiMoO4 nano-rods for excellent electro-catalytic performance in hydrogen evolution reactions. Mater. Lett. 257,. https://doi.org/10.1016/j.matlet.2019.126696 126696.

Alajmi, M.F., Ahmed, J., Hussain, A., Ahamad, T., Alhokbany, N., Amir, S., Ahmad, T., Alshehri, S.M., 2018. Green synthesis of Fe3O4 nanoparticles using aqueous extracts of Pandanus odoratissimus leaves for efficient bifunctional electrocatalytic activity. Appl. Nanosci. 8, 1427–1435. https://doi.org/10.1007/s13204-018-0795-8.

Alshehri, S.M., Ahmed, J., Ahamad, T., Alhokbany, N., Arunachalam, P., Al-Mayouf, A. M., Ahmad, T., 2018. Synthesis, characterization, multifunctional electrochemical (OGR/ORR/SCs) and photodegradable activities of ZnWO4 nanobricks. J. Sol-Gel Sci. Technol. 87, 137–146. https://doi.org/10.1007/s10971-018-4698-7.

AlShehri, S.M., Ahmed, J., Ahamad, T., Arunachalam, P., Ahmad, T., Khan, A., 2017. Bifunctional electro-catalytic performances of CoWO4 nanocubes for water redox reactions (OER/ORR). RSC Adv. 7, 45615–45623. https://doi.org/10.1039/C7RA07256B.

Balaji, S.S., Sathish, M., 2014. Supercritical fluid processing of nitric acid treated nitrogen doped graphene with enhanced electrochemical supercapacitance. RSC Adv. 4, 52256–52262. https://doi.org/10.1039/C4RA07820A.

Bera, S., Ghosh, S., Basu, R.N., 2018. Fabrication of Bi2S3/ZnO heterostructures: an excellent photocatalyst for visible-light-driven hydrogen generation and photoelectrochemical properties. New J. Chem. 42, 541–554. https://doi.org/10.1039/C7NJ03424E.

Callsen, G., Reparaz, J.S., Wagner, M.R., Kirste, R., Nenstiel, C., Hoffmann, A., Phillips, M.R., 2011. Phonon deformation potentials in wurtzite GaN and ZnO determined by uniaxial pressure dependent Raman measurements. Appl. Phys. Lett. 98, 61906. https://doi.org/10.1063/1.3554434.

Carenco, S., Portehault, D., Boissière, C., Mézailles, N., Sanchez, C., 2013. Nanoscaled metal borides and phosphides: recent developments and perspectives. Chem. Rev. 113, 7981–8065. https://doi.org/10.1021/cr400020d.

Chen, H.M., Chen, C.K., Liu, R.-S., Zhang, L., Zhang, J., Wilkinson, D.P., 2012. Nano-architecture and material designs for water splitting photoelectrodes. Chem. Soc. Rev. 41, 5654–5671. https://doi.org/10.1039/C2CS35019J.

Cherevko, S., Geiger, S., Kasian, O., Kulyk, N., Grote, J.-P., Savan, A., Shrestha, B.R., Merzlikin, S., Breitbach, B., Ludwig, A., Mayrhofer, K.J.J., 2016. Oxygen and hydrogen evolution reactions on Ru, RuO2, Ir, and IrO2 thin film electrodes in acidic and alkaline electrolytes: A comparative study on activity and stability. Catal. Today 262, 170–180. https://doi.org/10.1016/j.cattod.2015.08.014.

Desai, M.A., Vyas, A.N., Saratale, G.D., Sartale, S.D., 2019. Zinc oxide superstructures: Recent synthesis approaches and application for hydrogen production via photoelectrochemical water splitting. Int. J. Hydrogen Energy 44, 2091–2127. https://doi.org/10.1016/j.ijhydene.2018.08.042.

Elakkiya, R., Ramkumar, R., Maduraiveeran, G., 2019. Flower-like nickel-cobalt oxide nanomaterials as bi-functional catalyst for electrochemical water splitting. Mater. Res. Bull. 116, 98–105. https://doi.org/10.1016/j.materresbull.2019.04.016.

Fester, J., Makoveev, A., Grumelli, D., Gutzler, R., Sun, Z., Rodríguez-Fernández, J., Kern, K., Lauritsen, J.V., 2018. The structure of the cobalt oxide/Au catalyst interface in electrochemical water splitting. Angew. Chem. Int. Ed. 57, 11893–11897. https://doi.org/10.1002/anie.201804417.

Gao, P., Liu, Z., Sun, D.D., 2013. The synergetic effect of sulfonated graphene and silver as co-catalysts for highly efficient photocatalytic hydrogen production of ZnO nanorods. J. Mater. Chem. A 1, 14262–14269. https://doi.org/10.1039/C3TA13047A.

Hüner, B., Farsak, M., Telli, E., 2018. A new catalyst of AlCu@ZnO for hydrogen evolution reaction. Int. J. Hydrogen Energy 43, 7381–7387. https://doi.org/10.1016/j.ijhydene.2018.02.186.

Hwang, S.-H., Seo, H.-J., Kim, Y.K., Lim, S.K., 2016. Solar hydrogen production of ZnO horn electrodeposited on carbon film. Mater. Sci. Semicond. Process. 41, 226–232. https://doi.org/10.1016/j.mssp.2015.08.048.

Jain, I.P., 2009. Hydrogen the fuel for 21st century. Int. J. Hydrogen Energy 34, 7368–7378. https://doi.org/10.1016/j.ijhydene.2009.05.093.

Khatoon, S., Wani, I.A., Ahmed, J., Magdaleno, T., Al-Hartomy, O.A., Ahmad, T., 2013. Effect of high manganese substitution at ZnO host lattice using solvothermal method: Structural characterization and properties. Mater. Chem. Phys. 138, 519–528. https://doi.org/10.1016/j.matchemphys.2012.12.013.

Kumar, B., Kim, S.-W., 2012. Energy harvesting based on semiconducting piezoelectric ZnO nanostructures. Nano Energy 1, 342–355. https://doi.org/10.1016/j.nanoen.2012.02.001.

Kumar, S., Reddy, N.L., Kumar, A., Shankar, M.V., Krishnan, V., 2018. Two dimensional N-doped ZnO-graphitic carbon nitride nanosheets heterojunctions with enhanced photocatalytic hydrogen evolution. Int. J. Hydrogen Energy 43, 3988–4002. https://doi.org/10.1016/j.ijhydene.2017.09.113.

Kwak, I., Kwon, I.S., Kim, J., Park, K., Ahn, J.-P., Yoo, S.J., Kim, J.-G., Park, J., 2017. IrO2–ZnO hybrid nanoparticles as highly efficient trifunctional electrocatalysts. J. Phys. Chem. C 121, 14899–14906. https://doi.org/10.1021/acs.jpcc.7b03844.

Lehr, D., Luka, M., Wagner, M.R., Bügler, M., Hoffmann, A., Polarz, S., 2012. Band-Gap Engineering of Zinc Oxide Colloids via Lattice Substitution with Sulfur Leading to Materials with Advanced Properties for Optical Applications Like Full Inorganic UV Protection. Chem. Mater. 24, 1771–1778. https://doi.org/10.1021/cm300239q.

Ling, C., Zhou, L.Q., Jia, H., 2014. First-principles study of crystalline CoWO4 as oxygen evolution reaction catalyst. RSC Adv. 4, 24692–24697. https://doi.org/10.1039/C4RA03893B.

Liu, B., Shioyama, H., Akita, T., Xu, Q., 2008. Metal-Organic Framework as a Template for Porous Carbon Synthesis. J. Am. Chem. Soc. 130, 5390–5391. https://doi.org/10.1021/ja7106146.

Lonkar, S.P., Pillai, V., Abdala, A., Mittal, V., 2016. In situ formed graphene/ZnO nanostructured composites for low temperature hydrogen sulfide removal from natural gas. RSC Adv. 6, 81142–81150. https://doi.org/10.1039/C6RA08763A.

Matinise, N., Fuku, X.G., Kaviyarasu, K., Mayedwa, N., Maaza, M., 2017. ZnO nanoparticles via Moringa oleifera green synthesis: Physical properties & mechanism of formation. Appl. Surf. Sci. 406, 339–347. https://doi.org/10.1016/j.apsusc.2017.01.219.

Meyer, S., Nikiforov, A.V., Petrushina, I.M., Köhler, K., Christensen, E., Jensen, J.O., Bjerrum, N.J., 2015. Transition metal carbides (WC, Mo2C, TaC, NbC) as potential electrocatalysts for the hydrogen evolution reaction (HER) at medium temperatures. Int. J. Hydrogen Energy 40, 2905–2911. https://doi.org/10.1016/j.ijhydene.2014.12.076.

Mohan, R., Krishnamoorthy, K., Kim, S.-J., 2012. Enhanced photocatalytic activity of Cu-doped ZnO nanorods. Solid State Commun. 152, 375–380. https://doi.org/10.1016/j.ssc.2011.12.008.

Nojoumi, H., Dincer, I., Naterer, G.F., 2009. Greenhouse gas emissions assessment of hydrogen and kerosene-fueled aircraft propulsion. Int. J. Hydrogen Energy 34, 1363–1369. https://doi.org/10.1016/j.ijhydene.2008.11.017.

Nour, E.S., Nur, O., Willander, M., 2017. Zinc oxide piezoelectric nano-generators for low frequency applications. Semicond. Sci. Technol. 32, 64005. https://doi.org/10.1088/1361-6641/aa6bde.

Peng, C., Jin, J., Chen, G.Z., 2007. A comparative study on electrochemical co-deposition and capacitance of composite films of conducting polymers and carbon nanotubes. Electrochim. Acta 53, 525.

Peng, Y., Jiang, K., Hill, W., Lu, Z., Yao, H., Wang, H., 2019. Large-Scale, Low-Cost, and High-Efficiency Water-Splitting System for Clean H2 Generation. ACS Appl. Mater. Interfaces 11, 3971–3977. https://doi.org/10.1021/acsami.8b19251.

Qi, K., Cheng, B., Yu, J., Ho, W., 2017. Review on the improvement of the photocatalytic and antibacterial activities of ZnO. J. Alloy. Compd. 727, 792–820. https://doi.org/10.1016/j.jallcom.2017.08.142.

Rahman, W., Garain, S., Sultana, A., Middya, T.R., Mandal, D., 2018. Self-Powered Piezoelectric Nanogenerator Based on Wurtzite ZnO Nanoparticles for Energy Harvesting Application. Mater. Today:. Proc. 5, 9826–9830. https://doi.org/10.1016/j.matpr.2017.10.173.

Read, C.G., Callejas, J.F., Holder, C.F., Schaak, R.E., 2016. General strategy for the synthesis of transition metal phosphide films for electrocatalytic hydrogen and oxygen evolution. ACS Appl. Mater. Interfaces 8, 12798–12803. https://doi.org/10.1021/acsami.6b02352.

SoYoon, S., Ramadoss, A., Saravanakumar, B., Kim, S.J., 2014. Novel Cu/CuO/ZnO hybrid hierarchical nanostructures for non-enzymatic glucose sensor application. J. Electroanal. Chem. 717–718, 90–95. https://doi.org/10.1016/j.jelechem.2014.01.012.

Su, Y., Li, S., He, D., Yu, D., Liu, F., Shao, N., Zhang, Z., 2018. MOF-Derived Porous ZnO Nanocages/rGO/Carbon Sponge-Based Photocatalytic Microreactor for Efficient Degradation of Water Pollutants and Hydrogen Evolution. ACS Sustain. Chem. Eng. 6, 11989–11998. https://doi.org/10.1021/acssuschemeng.8b02287.

Suen, N.-T., Hung, S.-F., Quan, Q., Zhang, N., Xu, Y.-J., Chen, H.M., 2017. Electrocatalysis for the oxygen evolution reaction: recent development and future perspectives. Chem. Soc. Rev. 46, 337–365. https://doi.org/10.1039/C6CS00328A.

Sun, H., Yan, Z., Liu, F., Xu, W., Cheng, F., Chen, J., n.d. Self-Supported Transition-Metal-Based Electrocatalysts for Hydrogen and Oxygen Evolution. Advanced Materials 0, 1806326. https://doi.org/10.1002/adma.201806326.

Theerthagiri, J., Chandrasekaran, S., Salla, S., Elakkiya, V., Senthil, R.A., Nithyadharseni, P., Maiyalagan, T., Micheal, K., Ayeshamariam, A., Arasu, M.V.,

Al-Dhabi, Kim, H.-S., . Recent developments of metal oxide based heterostructures for photocatalytic applications towards environmental remediation. J. Solid State Chem. 267, 35–52. https://doi.org/10.1016/j.jssc.2018.08.006.

Yang, Y.-W., Liu, X.-H., Gao, E.-P., Feng, T.-T., Jiang, W.-J., Wu, J., Jiang, H., Sun, B., 2018. Self-template construction of nanoporous carbon nanorods from a metal–organic framework for supercapacitor electrodes. RSC Adv. 8, 20655–20660. https://doi.org/10.1039/C8RA03650K.

Yoo, H., Kahng, S., Kim, J.H., 2020. Z-scheme assisted ZnO/Cu2O-CuO photocatalysts to increase photoactive electrons in hydrogen evolution by water splitting. Sol. Energy Mater. Sol. Cells 204,. https://doi.org/10.1016/j.solmat.2019.110211 110211.

Zou, X., Zhang, Y., 2015. Noble metal-free hydrogen evolution catalysts for water splitting. Chem. Soc. Rev. 44, 5148–5180. https://doi.org/10.1039/C4CS00448E.